Supporting information

Two birds with one stone: Simultaneous adsorption and reduction of Cr(VI) in water by an engineered thiol group-perylene diimide covalent organic polymer

*Tao Jiang [a], Aokun Jia [a], Xin Zheng [a], Wenjie Guo [b], Zhi Luo [a], Qianyi Zuo [a], Jiahong Pan [c], Zhuoyu Ji [a *], Guixia Zhao [a]*

[a] College of Environmental Science and Engineering, North China Electric Power University, Beijing, 102206, P. R. China

[b] Department of Chemistry, Tsinghua University, Beijing, 100084, P. R. China

[c] State Key Laboratory of Featured Metal Materials and Life-Cycle Safety for Composite Structures, School of Resources, Environments and Materials, Guangxi University, Nanning 530004, China

[*] Corresponding author: Email: Zhuoyu Ji: jizhuoyu@ncepu.edu.cn

Text S1

The materials and reagents used in this study are shown in Table S1, and all reagents were used directly without further purification.

Table S1 Experimental materials and reagents.

Chemical reagent names	Molecular formula	Reagent purity	Manufacturers of reagents
3,4,9,10-Perylenetetracarboxylic acid dianhydride	$C_{24}H_8O_6$	GR	Leyan
2,5-Diamino-1,4-Benzenedithiophenol dihydrochloride	$C_6H_{10}Cl_2N_2S_2$	97%	Bide Pharmatech Co., Ltd
N,N-Dimethylformamide	C_3H_7NO	99.9%	Energy Chemical
Anhydrous zinc acetate	$C_4H_6O_4Zn$	99.99%	Macklin
Imidazole	$C_3H_4N_2$	99.72%	Bide Pharmatech Co., Ltd
Sodium chloride	NaCl	GR	Energy Chemical
Potassium chloride	KCl	GR	Energy Chemical
Calcium chloride	$CaCl_2$	GR	Energy Chemical
Calcium chloride	NaNO2	GR	Energy Chemical
Sodium sulfate	NaSO4	GR	Energy Chemical
Methanol	CH_4O	99.5%	Energy Chemical
sulfuric acid	H_2SO_4	AR	China National Pharmaceutical Group Corporation
Phosphoric acid	H_3PO_4	GR	Energy Chemical
Diphenylcarbazide	$C_{13}H_{14}N_4O$	GR	Energy Chemical
Acetone	C_3H_6O	AR	Aladdin
Humic acid	-	AR	Energy Chemical

Text S2

The Cr(VI) concentration was determined as follows: 1 mL of the sample to be tested was transferred into a 50 mL colorimetric tube and diluted to the mark with deionized water. Then, 0.5 mL of sulfuric acid solution (sulfuric acid to deionized water volume ratio of 1: 1) and 0.5 mL of phosphoric acid solution (phosphoric acid to deionized water volume ratio of 1: 1) were added and mixed thoroughly. Subsequently, 2 mL of the color-developing reagent (prepared by dissolving 0.20 g diphenylcarbazide in 50 mL acetone and diluting to 100 mL with water) was added. After thorough mixing, the solution was allowed to stand for 10 min for color development. The absorbance was then measured at 540 nm using a UV–visible spectrophotometer with a 30 mm cuvette, taking water as the reference. After subtracting the absorbance of the blank test, the Cr(VI) content was obtained from the calibration curve.

Text S3

(1) Effect of solution pH

To investigate the effect of solution pH on the adsorption capacity of Cr(VI) by PDI-DBD-SH, 15 mg of the adsorbent was weighed into a 50 mL centrifuge tube, followed by the addition of 30 mL of a 10 mg L^{-1} potassium dichromate solution. The suspension was then ultrasonicated for 5 - 10 min, and the pH of solution was adjusted to 3.0, 4.0, 5.0, 6.0, 7.0, 8.0, 9.0, and 10.0 using 0.1 mol L^{-1} hydrochloric acid and 0.1 mol L^{-1} sodium hydroxide solutions. After pH adjustment, all samples were placed on a thermostatic shaker and shaken for 12 h for reaching adsorption equilibrium. The suspensions were filtered through 0.22 μm aqueous membrane filters, and the Cr(VI) concentration was determined. The adsorption capacity of PDI-DBD-SH for Cr(VI) was then calculated according to Eq. (S1). All experiments were conducted in duplicate.

$$q_e = (C_0 - C_e) \times \frac{v}{m} \qquad \text{S(1)}$$

(2) Effect of coexisting ions

To investigate the effects of different coexisting ions on the adsorption capacity of Cr(VI) by PDI-DBD-SH, 15 mg of the adsorbent was weighed into a 50 mL centrifuge tube, followed by the addition of 15 mL of a 20 mg L^{-1} potassium dichromate solution and 15 mL of a 0.2 mol L^{-1} NaCl, KCl, or $CaCl_2$ solution (cations) or a 0.2 mol L^{-1} $NaNO_2$ or Na_2SO_4 solution (anions). The suspension was then ultrasonicated for 5 - 10 min, and the pH of the mixed solution were adjusted to 3.0 using 0.1 mol L^{-1} hydrochloric acid and 0.1 mol L^{-1} sodium hydroxide solutions. After pH adjustment, all samples were

placed on a thermostatic shaker and shaken for 12 h for reaching adsorption equilibrium. The suspensions were filtered through 0.22 μm aqueous membrane filters, and the Cr(VI) concentration was determined. All experiments were conducted in duplicate.

(3) Effect of coexisting organic matter

To investigate the effect of different concentrations of coexisting organic matter on the adsorption capacity of Cr(VI) by PDI-DBD-SH, 15 mg of the adsorbent was weighed into a 50 mL centrifuge tube, followed by the addition of 15 mL of a 20 mg L^{-1} potassium dichromate solution and 15 mL of humic acid solutions at concentrations of 10, 20, and 30 mg L^{-1}. The suspension was then ultrasonicated for 5 - 10 min, and the pH of the mixed solution was adjusted to 3.0 using 0.1 mol L^{-1} hydrochloric acid and 0.1 mol L^{-1} sodium hydroxide solutions. After pH adjustment, all samples were placed on a thermostatic shaker and shaken for 12 h for reaching adsorption equilibrium. The suspensions were filtered through 0.22 μm aqueous membrane filters, and the Cr(VI) concentration was determined. All experiments were conducted in duplicate.

(4) Adsorption isotherm experiments

To investigate the effect of different initial Cr(VI) concentrations on the adsorption capacity of Cr(VI) by PDI-DBD-SH, 15 mg of the adsorbent was weighed into a 50 mL centrifuge tube, followed by the addition of 30 mL potassium dichromate solutions with concentrations of 10, 20, 30, 40, and 50 mg L^{-1}. The pH of the potassium dichromate solutions was then adjusted to 3.0 using 0.1 mol L^{-1} hydrochloric acid and 0.1 mol L^{-1} sodium hydroxide solutions. After pH adjustment, all samples were placed on a thermostatic shaker and shaken for 12 h for reaching adsorption equilibrium. The suspensions were filtered through 0.22 μm aqueous membrane filters, and the Cr(VI) concentration was determined. All experiments were conducted in duplicate. The experimental data were fitted using Eqs. (S2) and (S3) to analyze the adsorption mechanisms.

Langmuir model equation:

$$q_e = \frac{K_L q_m C_e}{1+K_L C_e} \quad \text{S(2)}$$

Freundlich model equation:

$$q_e = K_f C_e^{\frac{1}{n}} \quad \text{S(3)}$$

Where q_e and C_e are the equilibrium adsorption capacity of the adsorbent at a given initial concentration

(mg g^{-1}) and the equilibrium concentration of Cr(VI) (mg L^{-1}), respectively. The q_m denotes the maximum adsorption capacity of the adsorbent. K_L (L g^{-1}) is the Langmuir constant, and K_f (L·mg/g·mg1/n) and 1/n are the fitting constants of the Freundlich model.

(5) Adsorption kinetics experiments

To investigate the effects of reaction time on the adsorption capacity of PDI-DBD-SH toward Cr(VI), 15 mg of the adsorbent was weighed into a 50 mL centrifuge tube, followed by the addition of 30 mL of a 10 mg L^{-1} potassium dichromate solution. After ultrasonic dispersion for 5 - 10 min, the pH of the system was adjusted to 3.0 using 0.1 mol L^{-1} hydrochloric acid and 0.1 mol L^{-1} sodium hydroxide solutions. After pH adjustment, all samples were placed on a thermostatic shaker for adsorption, and aliquots were withdrawn at 5, 15, 30, 60, 120, 180, and 240 min. The suspensions were filtered through 0.22 μm aqueous membrane filters, and the residual Cr(VI) concentration (C_t, mg L^{-1}) was determined. The adsorption capacity (q_t, mg g^{-1}) at specific time (t, min) was then calculated. The experimental data (q_t) - (t) were fitted using the pseudo-first-order kinetic model (Eq. (S4)), pseudo-second-order kinetic model (Eq. (S5)), and Elovich model (Eq. (S6)) to analyze the adsorption kinetics mechanisms.

Pseudo-first-order kinetic model equation:

$$\ln(q_e - q_t) = \ln q_e - K_1 t \qquad \text{S(4)}$$

Pseudo-second-order kinetic model equation:

$$t/q_t = t/q_e + \frac{1}{K_2 q_e^2} \qquad \text{S(5)}$$

Elovich model equation:

$$q_e = K_3 \ln t + a \qquad \text{S(6)}$$

Where q_e denotes the equilibrium adsorption capacity of the adsorbent at the given potassium dichromate concentration. q_t represents the adsorption capacity (mg g^{-1}) of the adsorbent at a given time (t, min). The K_1 and K_2 are the rate constants of the pseudo-first-order and pseudo-second-order kinetic models, respectively. and K_3 and a are the constants of the Elovich model.

(6) Application in real water systems

To evaluate the practical applicability of the adsorbent in real environmental systems, tap water and lake water solutions containing 10 mg L^{-1} potassium dichromate were prepared and reserved for use. In addition, a 10 mg L^{-1} potassium dichromate solution prepared with deionized water was used as a control.

Then, 15 mg of PDI-DBD-SH was added to a 50 mL centrifuge tube, followed by the addition of 30 mL of the 10 mg L^{-1} potassium dichromate solutions prepared with deionized water, tap water, and lake water, respectively. After ultrasonic mixing to ensure homogeneity, the solution pH was adjusted to 3.0. Following 12 h of adsorption, the suspensions were withdrawn, filtered through a 0.22 μm aqueous membrane filter, and the Cr(VI) concentration was determined.

(7) Recycling and regeneration experiments

Recycling and regeneration experiments were conducted under the same adsorption conditions described above. Briefly, 15 mg of PDI-DBD-SH was added to a 50 mL centrifuge tube containing 30 mL of 10 mg L^{-1} potassium dichromate solution, and the solution pH was adjusted to 3.0 after ultrasonic mixing. After adsorption for 12 h, the suspension was filtered through a 0.22 μm aqueous membrane filter, and the residual Cr(VI) concentration was determined. The used adsorbent was then regenerated by treating it with 0.1 M NaOH solution for 3 h to desorb the adsorbed chromium species. Subsequently, the material was thoroughly washed with a large amount of deionized water to remove residual NaOH and desorbed chromium species. The regenerated adsorbent was collected and dried in a vacuum oven at 60°C before being reused in the next adsorption cycle.

(8) Characterization methods

Powder X-ray diffraction (PXRD) patterns were recorded on a Rigaku Smart Lab SE diffractometer with a Cu Kα source, and instrumental deviation was corrected using small-angle X-ray scattering data from a Bruker D8 Advance diffractometer. The step size was 0.01°. Fourier transform infrared spectra (FT-IR) were recorded on a SHIMADZU IRTracer-100. Brunauer-Emmett-Teller (BET) surface areas were determined from N_2 adsorption/desorption isotherms collected at 77 K using a Micromeritics ASAP 2460 surface area analyzer. Scanning electron microscopy (SEM) images were acquired using a ZEISS GeminiSEM 360 scanning electron microscope. X-ray photoelectron spectroscopy (XPS) analyses were performed using a Thermo Scientific Nexsa G2 spectrometer equipped with a monochromated Al Kα X-ray source. Water contact angle (WCA) analyses were performed using a KRÜSS DSA25 standard drop shape analyzer at room temperature. Zeta potential measurements were performed using a Zetasizer Nano ZSE analyzer (Malvern Panalytical, UK) at room temperature.

(9) Computational Methods

The molecular structure optimization was carried to by using Gaussian 16W package based on DFT/6-

311g basis group and method. The electrostatic potential of PDI-DBD-SH was acquired by inputting chk. file of optimized structure into GaussView 6.0 package.

The DFT calculations with periodic boundary conditions were performed by Vienna Ab initio Simulation Package (VASP5.4.4) code [1]. The Perdew, Burke, and Ernzerhof (PBE) generalized gradient approximation (PBE-GGA) functionals were utilized to evaluate the exchange-correlation energies. VASPKIT, an input/output environment program in the VASP code, was used to manage the raw calculated data. The simulation was run with the setup of a 500 eV kinetic energy cut-off, and the K points grid for the Brillion zone was sampled using a 1 × 1 × 1 grid making gamma point centred regarding Monkhorst Pack Scheme, which was generated by VASPKIT. The GBs models were built in the shape of PDI-DBD-SH with Materials Studio 7.0 software. A vacuum space of 15 Å was created to eliminate interaction between slabs. The PDI-DBD-SH models with armchair and zig-zag edge configurations were constructed using cell sizes of 21.41×17.92 Å and 12.32×26.66 Å, respectively, the PDI-DBD-SH models with vacancy defect configuration was using cell size of 17.20×23.02 Å, all models were built in this study with the periodic boundary conditions. Geometry optimizations were carried out until the energies converged within 103 eV and the force on cach atom was less than -0.03 eV A-. We considered C atom sites without Hat the edge of a ~1 nm hexagonal hole configuration or armchair and zig-zag edges in the GBs model to represent the location of spin-containing defects. In contrast, H-saturated C atoms were selected as the location of non-spin-containing defects. Moreover, all calculations were spin-polarized. The density functional theory (DFT) calculations with periodic boundary conditions were performed by Vienna Ab initio Simulation Package (VASP 5.4.4). The projector augmented wave (PAW) methods were used to model core-valence electron interactions. The generalized gradient approximation (GGA) of the Perdue-Burke-Ernzerhof (PBE) version was used to describe the exchange-correlation interactions [1, 2]. VASPKIT, an input/output environment program in the VASP code, was used to manage the raw calculated data. The kinetic energy cutoff of the plane-wave was set to be 500 eV, and the K points grid for the Brillion zone was sampled using a 1 × 1 × 1 grid making gamma point centered regarding Monkhorst Pack Scheme, which was generated by VASPKIT. A vacuum space of 20 Å was created to eliminate interaction between slabs. Geometry optimizations were carried out until the energies converged within 10^{-5} eV and the force on each atom was less than 0.03 eV $Å^{-1}$. Moreover, The DFT-D3 method was used to describe the van der Waals interaction in this

work.

Table S2. Comparison of Cr(VI) adsorption capacities with other adsorbents.

Adsorbents	Adsorption capacity (mg/g)	References
AC-PSR	9.0	[3]
WB700	17.72	[4]
MBC/PPy	19.23	[5]
PS/PANi–Fe_3O_4	20.28	[6]
NZVI/GNS	21.72	[7]
NCB	23.16	[8]
GT-BC@nZVI/Cu	25.17	[9]
MCC/PANI-69 wt%	35.97	[10]
CPC-Al_{30}PMT	43.44	[11]
PDI-DBD-SH	53.42	This work
MB	55.00	[12]
BC900	64.13	[13]
nZVI/BC/CA	86.40	[14]

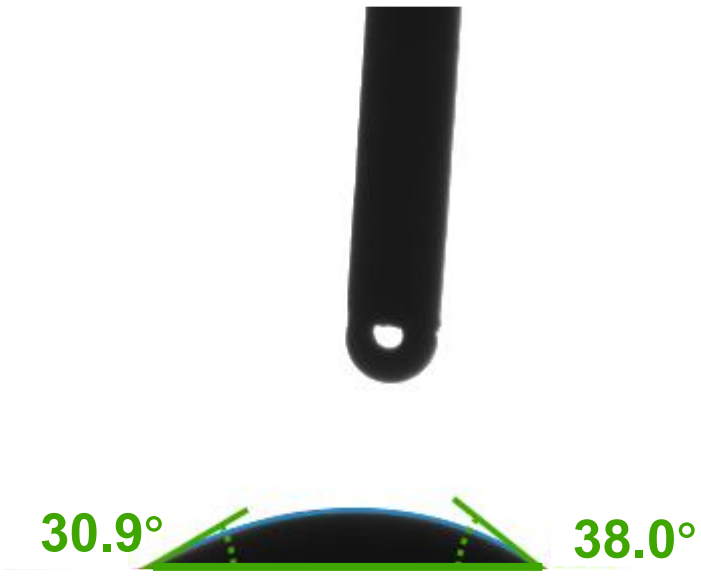

Fig. S1. The contact angle (10 s) of PDI-DBD-SH.

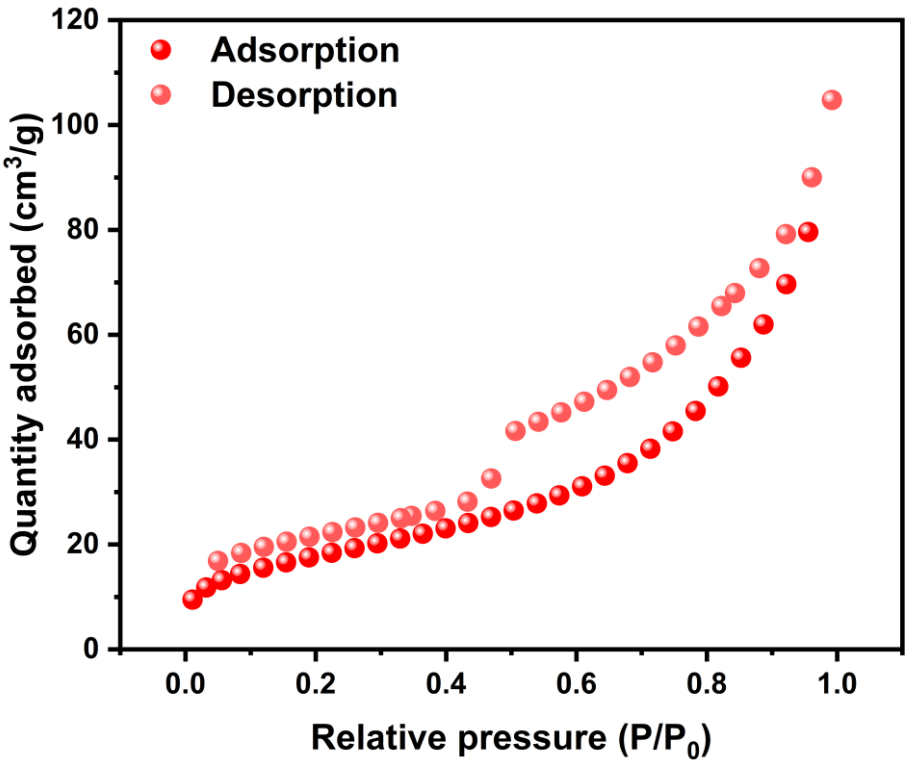

Fig. S2. N_2 adsorption–desorption isotherm of PDI-DBD-SH.

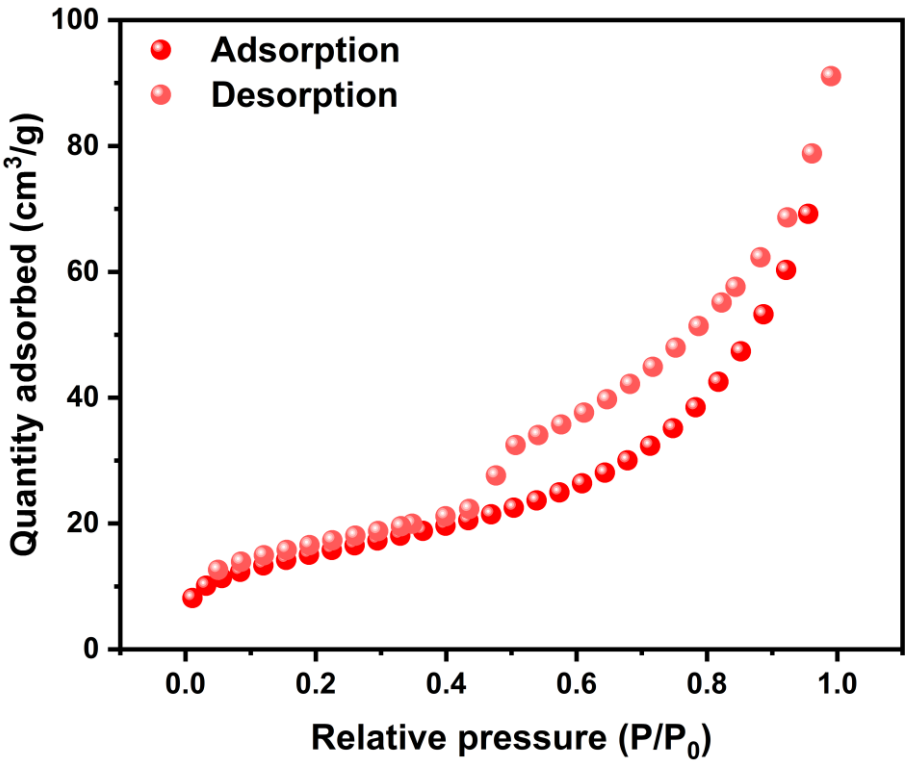

Fig. S3. N_2 adsorption–desorption isotherm of PDI-DBD-SH after Cr(VI) adsorption.

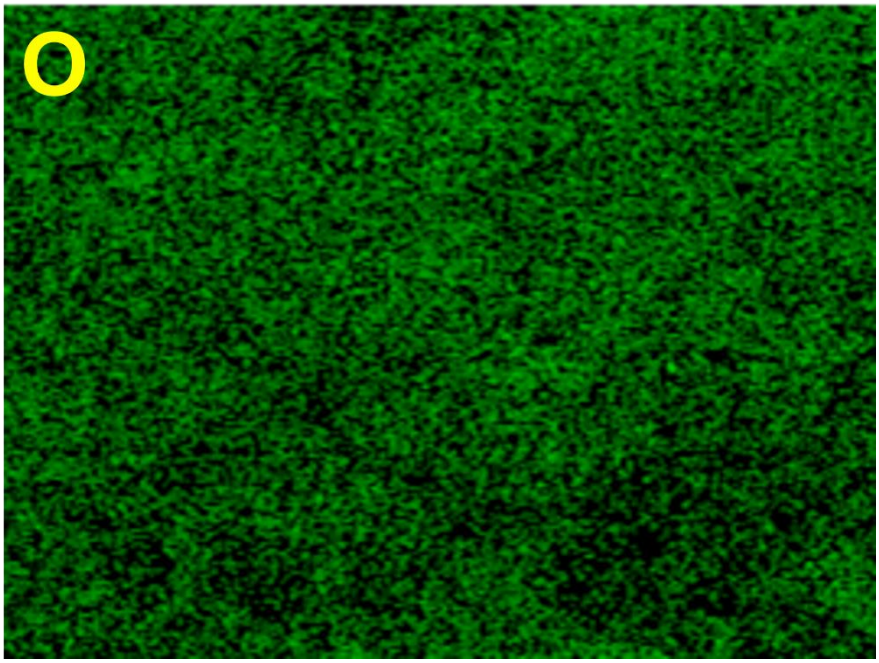

Fig. S4. EDS elemental mapping of PDI-DBD-SH after adsorption of aqueous Cr(VI).

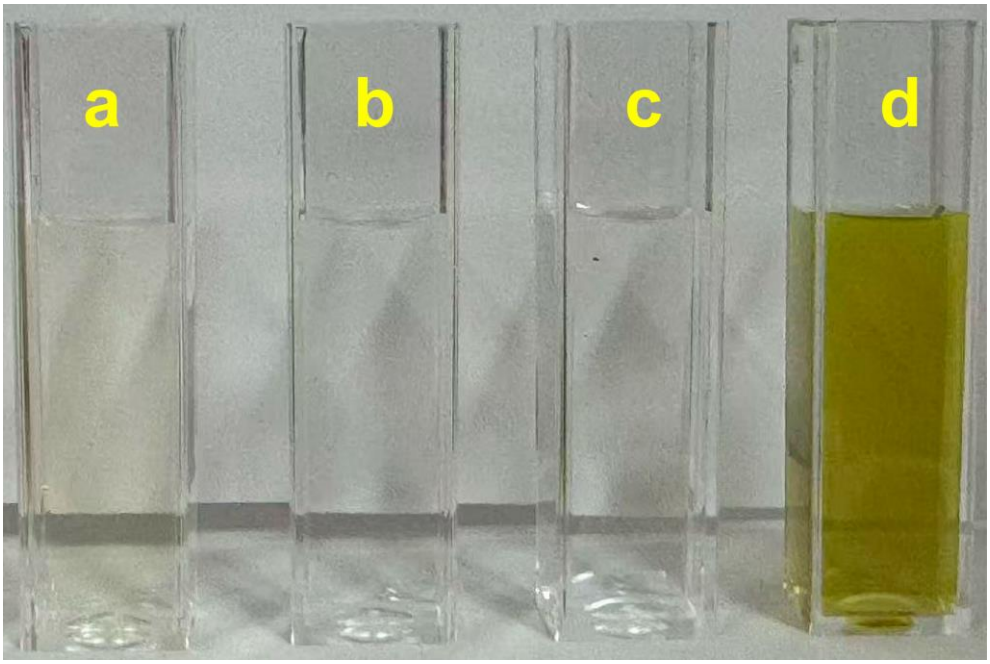

Fig. S5. (a) 10 mg L^{-1} $K_2Cr_2O_7$ solution. (b) Solution after Cr(VI) adsorption by PDI-DBD-SH. (c) Post–adsorption solution adjusted with 0.1 M NaOH. (d) Desorption solution obtained after treating Cr-loaded PDI-DBD-SH with 0.1 M NaOH.

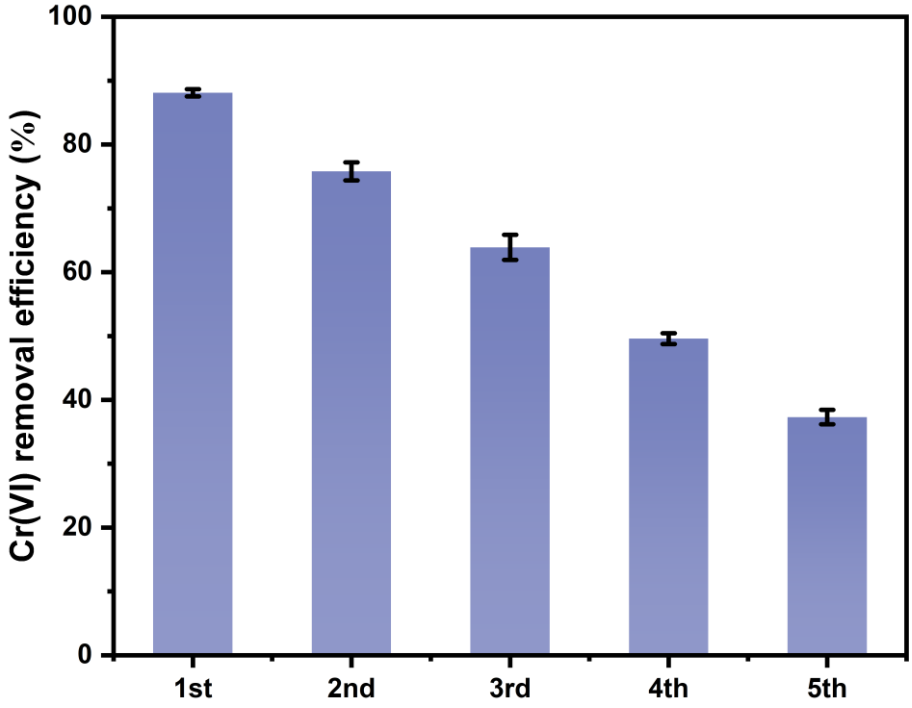

Fig. S6. Recycling performance of PDI-DBD-SH for Cr(VI) adsorption.

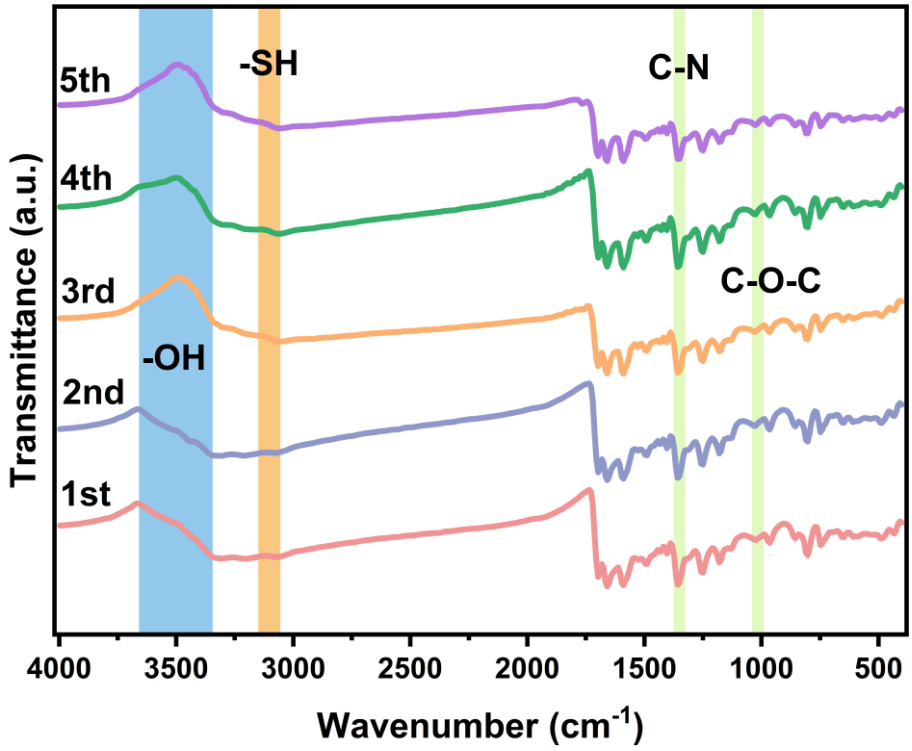

Fig. S7. FTIR spectra of PDI-DBD-SH during five adsorption–desorption cycles.

References:

1. G. Kresse and J. Furthmüller, *Comput. Mater. Sci*, 1996, **6**, 15-50.
2. J. P. Perdew, K. Burke and M. Ernzerhof, *Phys. Rev. Lett.*, 1996, **77**, 3865-3868.
3. S. Mortazavian, A. Saber, J. Hong, J.-H. Bae, D. Chun, N. Wong, D. Gerrity, J. Batista, K. J. Kim and J. Moon, *J. Ind. Eng. Chem.*, 2019, **69**, 196-210.
4. J. Wan, F. Liu, G. Wang, W. Liang, C. Peng, W. Zhang, K. Lin and J. Yang, *Bioresour. Technol.*, 2021, **337**, 125382.
5. Y. Yang, N. Chen, C. Feng, M. Li and Y. Gao, *Colloids Surf., A*, 2018, **556**, 201-209.
6. M. K. Debnath, M. A. Rahman, H. Minami, M. M. Rahman, M. A. Alam, M. K. Sharafat, M. K. Hossain and H. Ahmad, *J. Appl. Polym. Sci.*, 2019, **136**, 47524.
7. X. Li, L. Ai and J. Jiang, *Chem. Eng. J.*, 2016, **288**, 789-797.
8. T. L. Nguyen, A. Ayub, A. Anam, A. M. Aljuwayid, S. W. Alwash, R. Abbass, A. A. K. Ruhaima, E. Potrich, M. Sillanpaa, S. Gul, R. Alshammari, S. Ullah, K. Ahmad and H. H. Pham Thi, *J. Environ. Chem. Eng.*, 2023, **11**, 110445.
9. T. Li, F. Zhu, W. Liang, G. Hu, X. Deng, Y. Xue and J. Guan, *Process Safety and Environmental Protection*, 2022, **167**, 629-640.
10. L. Dewa, S. M. Tichapondwa and W. Mhike, *RSC Adv.*, 2024, **14**, 6603-6616.
11. X. Zou, F. Xiao, S. Liu, X. Cao, L. Li, M. Chen, L. Dong, X. Lyu and Y. Gai, *J. Water Process Eng.*, 2020, **37**, 101348.
12. S. Liang, S. Shi, H. Zhang, J. Qiu, W. Yu, M. Li, Q. Gan, W. Yu, K. Xiao, B. Liu, J. Hu, H. Hou and J. Yang, *Sci. Total Environ.*, 2019, **695**, 133886.
13. Y. Qiu, Q. Zhang, B. Gao, M. Li, Z. Fan, W. Sang, H. Hao and X. Wei, *Environ. Pollut.*, 2020, **265**, 115018.
14. Z. Wan, D. Cho, D. C. W. Tsang, M. Li, T. Sun and F. Verpoort, *Environ. Pollut.*, 2019, **247**, 410-420.